Journal of Nuclear Medicine, published on December 5, 2019 as doi:10.2967/jnumed.119.236885

Brief Communication

^{11}C-Methionine PET Identifies Astroglia Involvement in Heart-Brain Inflammation Networking after Acute Myocardial Infarction

Pablo Bascuñana[1], Annika Heß[1], Tobias Borchert[1], Yong Wang[2],

Kai C. Wollert[2], Frank M. Bengel[1], James T. Thackeray[1]

[1]Department of Nuclear Medicine, and

[2]Molecular and Translational Cardiology, Department of Cardiology and Angiology,

Hannover Medical School, Hannover, Germany

Brief Title: Imaging Astroglia after Infarction

Total Word Count: 2497

Corresponding Author:
James T Thackeray, PhD
Junior Research Group Leader
Translational Cardiovascular Molecular Imaging
Department of Nuclear Medicine
Hannover Medical School
Tel. +49 511/532.3358
Fax. +49 511/532.3761
Thackeray.James@mh-hannover.de

Sources of Funding: This work was supported by the German Research Foundation (DFG; grant Th2161/1-1 (JTT), KFO311 (FMB)).

ABSTRACT

Acute myocardial infarction (MI) triggers a local and systemic inflammatory response. We recently showed microglia involvement using TSPO imaging. Here, we evaluate whether ^{11}C-methionine provides further insights into heart-brain inflammation networking.

Methods: Male Bl6N mice underwent permanent coronary artery ligation followed by ^{11}C-methionine PET at 3 and 7 days (n=3). In subgroups, leukocyte homing was blocked by integrin antibodies (n=5). The cellular substrate for PET signal was identified using brain section immunostaining.

Results: ^{11}C-methionine uptake peaked in the MI region at d3 (5.9±0.9vs 2.4±0.5 %ID/cc), decreasing to control level by d7 (4.3±0.6 %ID/cc). Brain uptake was proportional to cardiac uptake ($r=0.47, p<0.05$), peaking also at d3 (2.9±0.4vs 2.4±0.3 %ID/cc) and returning to baseline at d7 (2.3±0.4 %ID/cc). Integrin blockade reduced uptake at every time point. Immunostaining at d3 revealed co-localization of the L-type amino acid transporter with GFAP-positive astrocytes but not CD68-positive microglia.

Conclusions: PET imaging with ^{11}C-methionine specifically identifies an astrocyte component, enabling further dissection of the heart-brain axis in post MI inflammation.

Key Words: Myocardial infarction, inflammation, PET, methionine, astroglia

Patients with cardiovascular disease bear increased risk of dementia, including Alzheimer's disease (*1-3*). Among various underlying factors, inflammation has been postulated as a link between cardiac injury and neurodegeneration (*4-6*). Recently, TSPO-targeted whole-body imaging confirmed the presence of concomitant cerebral microglia activation in the acute stages after myocardial infarction (MI) in mice and humans (*7*). Neuroinflammation, while implicated in the development of Alzheimer's dementia (*8*), is difficult to characterize using conventional blood testing or biopsy. Hence, noninvasive methods to characterize early activation of the heart-brain axis after cardiac damage are desirable.

Several radiotracers have been recently characterized for inflammation imaging, including ^{11}C-methionine, which is routinely used for clinical glioma imaging (*9*). After MI, ^{11}C-methionine robustly accumulates in pro-inflammatory leukocytes (*10,11*). Here, we hypothesize that whole-body ^{11}C-methionine PET may provide insights into heart-brain inflammation networking after MI that are complementary to those obtained previously with TSPO-targeted imaging.

MATERIALS AND METHODS

Animals. Adult male C57Bl/6 mice (n=34; Charles River Laboratories, Sulzfeld, Germany) were housed under standardized environmental conditions with free access to standard laboratory diet and water. All experiments were in accordance with the guidelines of the European Directive 2013/63/EU and German national laws, and with the approval of regional authorities.

Experimental model. Mice underwent coronary artery ligation (n=31) as described (*10*). A subgroup of animals (n=17) was treated with an anti-integrin antibody cocktail consisting of anti-CD11a (lymphocyte function-associated antigen-1, clone M17/4), anti-CD11b (macrophage-1 antigen, clone M1/70) and anti CD49d (very late antigen-4, clone PS/2), injected i.p. 2h before surgery and again 4d after MI, as described (*10*). These therapeutic antibodies interfere with leukocyte rolling and extravasation, reducing the recruitment of granulocytes, monocytes, and macrophages to the infarct territory (*12*). Following recovery, ^{11}C-methionine PET was conducted at 3 and 7d after MI.

Radiochemistry. ^{11}C-Methionine was synthesized as previously described by S-methylation of S-benzyl-homocysteine (*13*), yielding high radiochemical purity (>98%) and specific activity (>10GBq/μmol).

Small animal PET. Whole-body ^{11}C-methionine scans were acquired using an Inveon scanner (Siemens, Knoxville, TN) under isoflurane anesthesia and monitoring of body temperature, breathing frequency and heart rate. Injected dose was 17.2±5.4 MBq of ^{11}C-methionine. External source transmission scans were acquired for attenuation correction. Dynamic images (30min) were reconstructed using an ordered subset expectation maximization fast maximum a posteriori algorithm (OSEM3D/fastMAP, 2 iterations OSEM in 16 subsets, 18 iterations MAP, β=0.01). The reconstruction resulted in voxel sizes of 0.78×0.78×0.80 mm.

Image analysis. Using Pmod 3.7 software (Pmod Technologies, Zürich, Switzerland), brain PET images were automatically co-registered to individual CT images and CT was then fused to a MRI T2 template (*14*). PET images were then co-registered to the MRI template and a VOI template (*15*) was applied. Mean uptake normalized to the injected dose (%ID/cc) of each VOI was calculated. Cardiac and peripheral organ uptake

(i.e. liver, bone marrow, and thymus) was analyzed using Inveon Research Workplace as previously described (*10*).

Immunohistochemistry. Untreated (n=8) and anti-integrin treated (n=8) animals were sacrificed 3 and 7 days after MI. Brains were removed, snap-frozen and sliced in a cryostat (14µm). Fluoroimmunohistology targeting glial fibrillary acidic protein (GFAP) of astrocytes, CD68 of microglia and large neutral amino acid transporter (LAT-1) were performed. Thawed brain sections were fixed in acetone, blocked with horse serum (10% in PBS) and incubated with the primary antibodies (AlexaFluor488 anti-GFAP or AlexaFluor-488 anti-CD68 and AlexaFluor-647 anti-mouse CD98; Biolegend) for 60min. Slides were then washed with PBS, incubated with DAPI solution, washed again and coverslipped using fluorescence mounting medium (FluoreGuard, Dianova). Brain slices were analyzed using an epifluorescence confocal microscope. Fluorescence signal for GFAP, CD68 and LAT-1 was quantified in dorsal hippocampus and thalamus.

Statistics. Differences in imaging studies were analyzed by non-parametric Kruskal-Wallis test followed by post hoc test with selected comparisons. Fluorescence immunostaining results were compared by two-sided two-sample t-test. Data are presented as mean ± standard deviation (SD). Differences were considered statistically significant for $p<0.05$.

RESULTS

Serial PET demonstrated increased ^{11}C-methionine accumulation in the infarct territory at 3d after MI which declined to the level of healthy controls by 7d (Fig 1A,B). A concomitant elevation of ^{11}C-methionine signal was evident in the whole brain at 3d. This difference was reduced at 7d, similar to the heart (Fig 1A,D). Statistical parametric

mapping revealed the prominent signal increase in hypothalamus, hippocampus and dorsal thalamus regions (Fig 1C). The systemic immune response was evident, with a modest elevation of ^{11}C-methionine accumulation in bone marrow and thymus, reaching maximum at 3d post-MI (Fig 1E).

Anti-integrin antibody pretreatment led to significant decline in cardiac ^{11}C-methionine accumulation at 3d (Fig 1A,B). Uptake in the brain was comparably decreased, both in whole brain and in the regions of most pronounced elevation (Fig 1A,D). Hepatic ^{11}C-methionine uptake was not affected by anti-integrin treatment (11.7±2.0 vs 10.9±1.2%ID/g, p=NS), supporting interference with leukocyte extravasation over depletion. Overall, we found a good correlation between brain ^{11}C-methionine uptake and uptake in the MI territory ($r=0.47$, $p<0.05$).

Brain tissue immunostaining identified elevated density of GFAP-positive astrocytes in the hippocampus at 3d after MI compared to integrin-treated animals (596±141 vs 350±136; p=0.033; Fig 2). CD68-positive microglia were also present in cortex around the hipoocampus (Fig 2). LAT-1 as the substrate for methionine uptake was visualized at 3d and 7d post-MI, and attenuated by anti-integrin treatment (p=0.052, Fig 2B). Of note, LAT-1 did not colocalize with CD68-positive microglia (Fig 2A). Conversely, co-immunostaining demonstrated colocalization of LAT-1 with GFAP (Fig 2A).

DISCUSSION

Recent studies have emphasized the interconnection between the heart and the brain following ischemic damage. In the present study, we expand our prior observation of heart-brain inflammation networking using TSPO-targeted imaging, by using an alternative

targeted radiotracer of inflammation, ^{11}C-methionine. We demonstrate that ^{11}C-methionine uptake is elevated in brain early after myocardial infarction. Moreover, we identified expression of the L-type amino acid transporter particularly in GFAP-positive astrocytes, suggesting that ^{11}C-methionine identifies an astrocyte-driven component of neuroinflammation after acute myocardial infarction, which is different from the microglia component analyzed by TSPO imaging in our prior work (*7*).

^{11}C-methionine is widely used for glioma imaging, and is suitable for imaging inflammatory conditions in brain (*9,16,17*). We and others reported selective accumulation of ^{11}C-methionine by pro-inflammatory leukocytes within the infarct region after acute MI (*10,11*). The present study is the first to show that increased ^{11}C-methionine cardiac uptake is paralleled by increased brain uptake early after MI. Statistical parametric mapping points to hippocampus as one the most affected regions, which is implicated in systemic inflammation and may lead to impaired neurogenesis and memory deficits (*18,19*). ^{18}F-FDG uptake in the amygdala has been suggested as a contributing factor to atherosclerotic plaque inflammation and major adverse cardiac events (*20*). While quantitative analysis of murine amygdala is beyond the resolution of the PET camera, a tendency for increased amino acid metabolism was also identified in the present study.

Immunohistochemistry suggests increased LAT-1 in activated astrocytes but not CD68-positive microglia as the source of ^{11}C-methionine signal. This pattern is distinct from TSPO-ligand ^{18}F-GE180, which co-localized with microglia but not astroglia (*7*). The imaging time course suggests early neuroinflammatory astrocyte activity preceding microglia activation after MI, as methionine signal recovers to baseline at maximal microglial activation (*7*). Reactive astrocytes can be neurotoxic, producing reactive oxygen species and inflammatory cytokines. They also express high levels of amyloid precursor

proteins (*21*). As such, MI-induced astrocytic activation may lead to amyloid-β production and further neuroinflammation, a vicious cycle which may promote Alzheimer's disease pathology (*22,23*). While modestly higher astrocyte staining could be regionally identified, both histology and PET imaging suggest a global brain response to MI. Statistical parametric mapping suggests preferential involvement of specific brain regions, but requires dedicated regional analysis with higher-resolution techniques.

Application of an anti-integrin cocktail to inhibit cardiac leukocyte infiltration (*10*) also lowered brain ^{11}C-methionine uptake, but did not affect other peripheral organs. Anti-integrin antibody therapy impairs the rolling and extravasation of neutrophils, monocytes, and macrophages, without direct impact on leukocyte numbers (*24*). Similar to the PET signal, brain GFAP and LAT-1 were reduced, suggesting attenuated astrocyte activation, whereas CD68-positive microglia were unaffected. These findings suggest astrocyte activation after MI is directly linked to infarct-induced inflammation, and may point to pro-inflammatory cytokines as the cause of astrocytic activation. Neutrophils and pro-inflammatory monocytes, which exhibit high methionine uptake (*10*), appear to influence astrocyte activation. In contrast, peak microglial activation occurred slightly later (*7*) and did not decrease with the anti-integrin cocktail, suggesting that microglia response to additional factors.

CONCLUSION

Methionine may delineate the astrocyte component of neuroinflammation after MI, which may be complementary to microglial imaging by TSPO-targeted tracers. The temporal profile of these distinct components may guide therapeutic interventions to improve neurologic outcomes after MI. Further dedicated studies are warranted to delineate the precise role of astrocytes in relation to microglial activation and cognitive impairment.

Molecular imaging provides a multi-tracer toolbox to assess specific components of the heart-brain inflammatory axis.

DISCLOSURE

The authors report no conflicts of interest. This work was supported by grants of the German Research Foundation (DFG) to Drs. Bengel (KFO311) and Thackeray (Th2161/1-1).

KEY POINTS

Question: Can ^{11}C-methionine identify heart-brain inflammation networking after myocardial infarction?

Pertinent Findings: Peak brain signal occurs at day 3 after myocardial infarction, parallels peak myocardial inflammation, and is associated with activated astroglia (which is in contrast to previously used TSPO imaging that identifies microglia). **Translational Implications:** Characterization of distinct immune-metabolic tissue patterns will help in the development of anti-inflammatory, regenerative therapies.

REFERENCES

1. Breteler MM, Claus JJ, Grobbee DE, Hofman A. Cardiovascular disease and distribution of cognitive function in elderly people: the Rotterdam Study. *BMJ.* 1994;308:1604-1608.

2. Luchsinger JA, Reitz C, Honig LS, Tang MX, Shea S, Mayeux R. Aggregation of vascular risk factors and risk of incident Alzheimer disease. *Neurology.* 2005;65:545-551.

3. Qiu C, Winblad B, Marengoni A, Klarin I, Fastbom J, Fratiglioni L. Heart failure and risk of dementia and Alzheimer disease: a population-based cohort study. *Arch Intern Med.* 2006;166:1003-1008.

4. Nelson AR, Sweeney MD, Sagare AP, Zlokovic BV. Neurovascular dysfunction and neurodegeneration in dementia and Alzheimer's disease. *Biochim Biophys Acta.* 2016;1862:887-900.

5. de Roos A, van der Grond J, Mitchell G, Westenberg J. Magnetic Resonance Imaging of Cardiovascular Function and the Brain: Is Dementia a Cardiovascular-Driven Disease? *Circulation.* 2017;135:2178-2195.

6. Walker KA, Power MC, Gottesman RF. Defining the Relationship Between Hypertension, Cognitive Decline, and Dementia: a Review. *Curr Hypertens Rep.* 2017;19:24.

7. Thackeray JT, Hupe HC, Wang Y, et al. Myocardial Inflammation Predicts Remodeling and Neuroinflammation After Myocardial Infarction. *J Am Coll Cardiol.* 2018;71:263-275.

8. Krstic D, Knuesel I. Deciphering the mechanism underlying late-onset Alzheimer disease. *Nat Rev Neurol.* 2013;9:25-34.

9. Glaudemans AW, Enting RH, Heesters MA, et al. Value of 11C-methionine PET in imaging brain tumours and metastases. *Eur J Nucl Med Mol Imaging.* 2013;40:615-635.

10. Thackeray JT, Bankstahl JP, Wang Y, Wollert KC, Bengel FM. Targeting Amino Acid Metabolism for Molecular Imaging of Inflammation Early After Myocardial Infarction. *Theranostics.* 2016;6:1768-1779.

11. Taki J, Wakabayashi H, Inaki A, et al. 14C-Methionine uptake as a potential marker of inflammatory processes after myocardial ischemia and reperfusion. *J Nucl Med.* 2013;54:431-436.

12. Kempf T, Zarbock A, Widera C, et al. GDF-15 is an inhibitor of leukocyte integrin activation required for survival after myocardial infarction in mice. *Nat Med.* 2011;17:581-588.

13. Langstrom B, Antoni G, Gullberg P, et al. Synthesis of L- and D-[methyl-11C]methionine. *J Nucl Med.* 1987;28:1037-1040.

14. Ma Y, Hof PR, Grant SC, et al. A three-dimensional digital atlas database of the adult C57BL/6J mouse brain by magnetic resonance microscopy. *Neuroscience.* 2005;135:1203-1215.

15. Mirrione MM, Schiffer WK, Fowler JS, Alexoff DL, Dewey SL, Tsirka SE. A novel approach for imaging brain-behavior relationships in mice reveals unexpected metabolic patterns during seizures in the absence of tissue plasminogen activator. *Neuroimage.* 2007;38:34-42.

16. Hashimoto S, Inaji M, Nariai T, et al. Usefulness of [(11)C] Methionine PET in the Differentiation of Tumefactive Multiple Sclerosis from High Grade Astrocytoma. *Neurol Med Chir (Tokyo).* 2019;59:176-183.

17. Parente A, van Waarde A, Shoji A, et al. PET Imaging with S-[(11)C]Methyl-L-Cysteine and L-[Methyl-(11)C]Methionine in Rat Models of Glioma, Glioma Radiotherapy, and Neuroinflammation. *Mol Imaging Biol.* 2018;20:465-472.

18. Chesnokova V, Pechnick RN, Wawrowsky K. Chronic peripheral inflammation, hippocampal neurogenesis, and behavior. *Brain Behav Immun.* 2016;58:1-8.

19. Murray C, Sanderson DJ, Barkus C, et al. Systemic inflammation induces acute working memory deficits in the primed brain: relevance for delirium. *Neurobiol Aging.* 2012;33:603-616.e603.

20. Tawakol A, Ishai A, Takx RA, et al. Relation between resting amygdalar activity and cardiovascular events: a longitudinal and cohort study. *Lancet.* 2017;389:834-845.

21. Frost GR, Li YM. The role of astrocytes in amyloid production and Alzheimer's disease. *Open Biol.* 2017;7.

22. Rodriguez-Vieitez E, Saint-Aubert L, Carter SF, et al. Diverging longitudinal changes in astrocytosis and amyloid PET in autosomal dominant Alzheimer's disease. *Brain.* 2016;139:922-936.

23. Scholl M, Carter SF, Westman E, et al. Early astrocytosis in autosomal dominant Alzheimer's disease measured in vivo by multi-tracer positron emission tomography. *Sci Rep.* 2015;5:16404.

24. Li W, Nava RG, Bribriesco AC, et al. Intravital 2-photon imaging of leukocyte trafficking in beating heart. *J Clin Invest.* 2012;122:2499-2508.

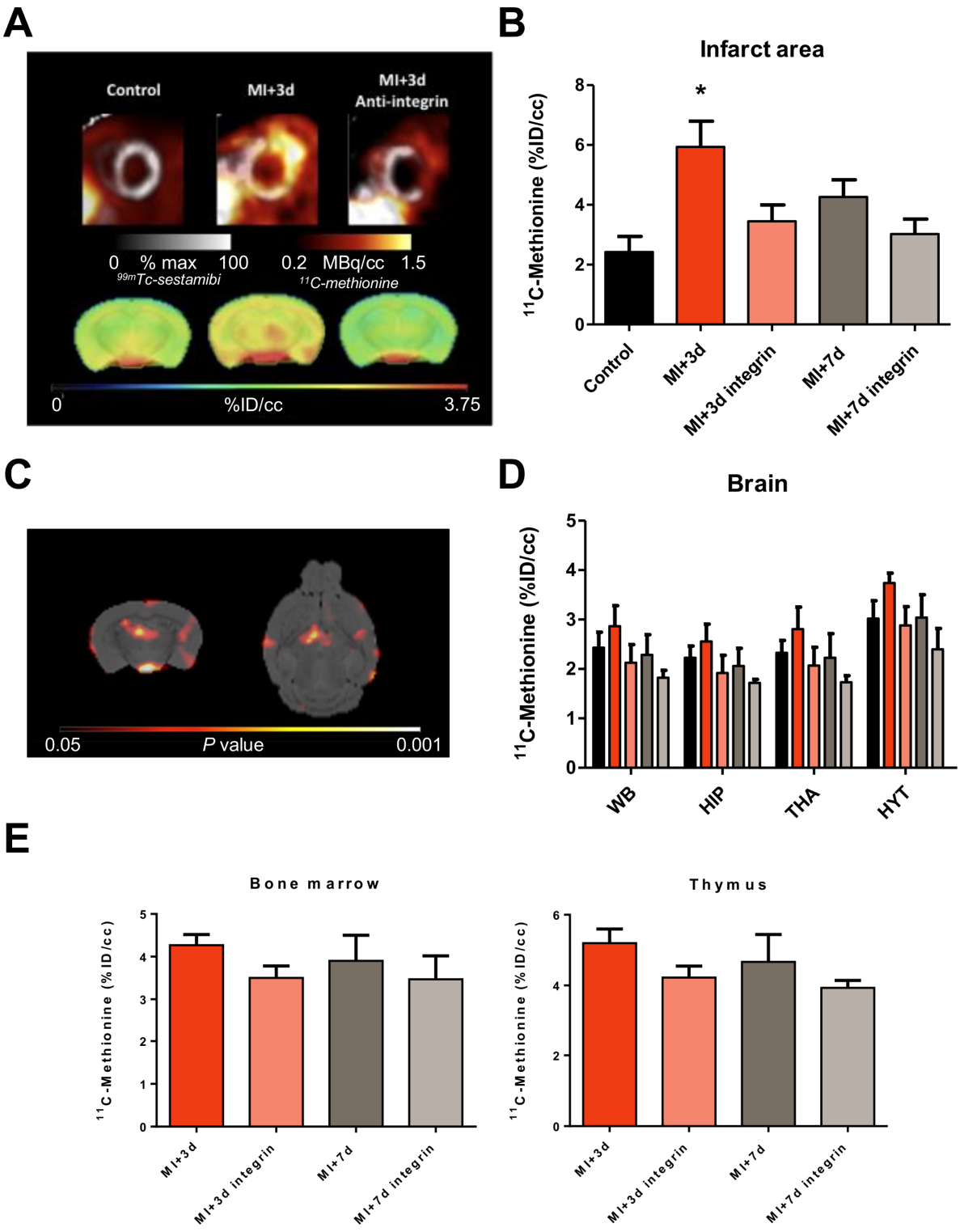

Figure 1. ^{11}C-Methionine uptake in heart and brain in control mice and after MI. (A) Representative cardiac and brain ^{11}C-methionine uptake in control and 3d after MI untreated and treated animals. (B) Semi-quantitative analysis of ^{11}C-

methionine uptake shows increased uptake in the infarct area and (D) brain regions (WB, whole brain; HIP, hippocampus; THA, thalamus; HYT, hypothalamus) at 3d after MI. (C) SPM t-map showing significant higher voxels in MI+3d vs control animals. (E) Semi-quantitative analysis of ^{11}C-methionine uptake in hematopoietic organs bone marrow and thymus (* $p<0.05$ to control).

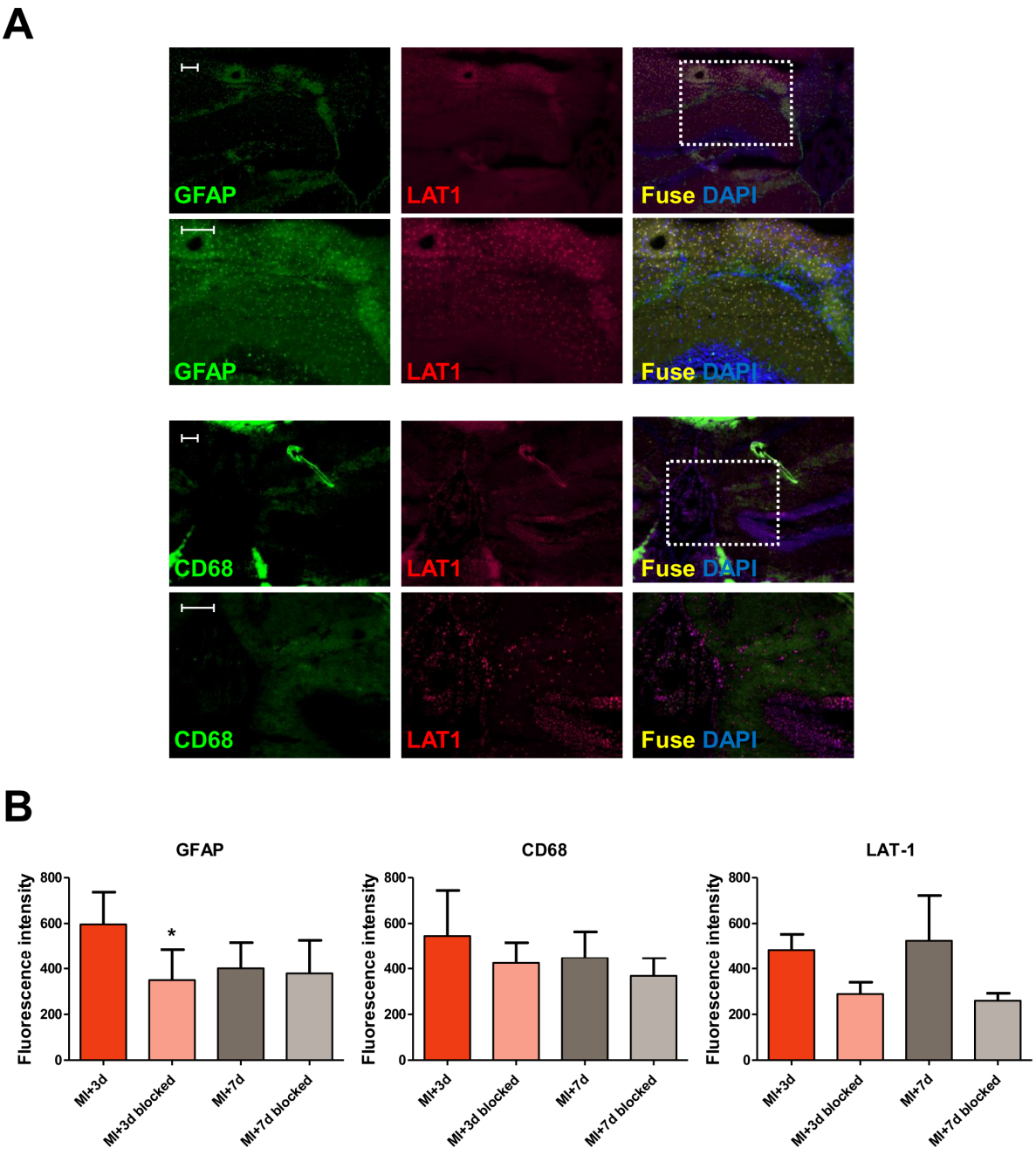

Figure 2. Immunostaining identifies astrocytes (GFAP), microglia (CD68) and amino acid transporter (LAT-1) in MI treated and untreated animals at 3 and 7d. (A) Merged images show co-localization of LAT-1 and GFAP (upper row) but not with CD68 (lower row) in hippocampus 3d after MI. Scale bar = 50µm. (B)

Semi-quantitative analysis of GFAP, CD68 and LAT-1 fluorescence intensity in hippocampus (* $p<0.05$ to control).